J Geod (2017) 91:1299–1311
DOI 10.1007/s00190-017-1026-x

ORIGINAL ARTICLE

Contribution of solar radiation and geomagnetic activity to global structure of 27-day variation of ionosphere

Yibin Yao[1] · **Changzhi Zhai**[1] · **Jian Kong**[2] · **Lei Liu**[1]

Received: 13 December 2016 / Accepted: 6 April 2017 / Published online: 19 April 2017

Abstract Twenty-seven-day variation caused by solar rotation is one of the main periodic effects of solar radiation influence on the ionosphere, and there have been many studies on this periodicity using peak electron density N_mF_2 and solar radio flux index F10.7. In this paper, the global electron content (GEC) and observation of Solar EUV Monitor (SEM) represent the whole ionosphere and solar EUV flux, respectively, to investigate the 27-day variation. The 27-day period components of indices (GEC_{27}, SEM_{27}, $F10.7_{27}$, Ap_{27}) are obtained using Chebyshev band-pass filter. The comparison of regression results indicates that the index SEM has higher coherence than F10.7 with 27-day variation of the ionosphere. The regression coefficients of SEM_{27} varied from 0.6 to 1.4 and the coefficients of Ap_{27} varied from −0.6 to 0.3, which suggests that EUV radiation seasonal variations are the primary driver for the 27-day variations of the ionosphere for most periods. TEC map grid points on three meridians where IGS stations are dense are selected for regression, and the results show that the contribution of solar EUV radiation is positive at all geomagnetic latitudes and larger than geomagnetic activity in most latitudes. The contribution of geomagnetic activity is negative at high geomagnetic latitude, increasing with decreasing geomagnetic latitudes, and positive at low geomagnetic latitudes. The global structure of 27-day variation of ionosphere is presented and demonstrates that there are two zonal anomaly regions along with the geomagnetic latitudes lines and two peaks in the north of Southeast Asia and the Middle Pacific where TEC_{27} magnitude values are notably larger than elsewhere along zonal anomaly regions.

Keywords 27-day variation in ionosphere · Solar radiation · Geomagnetic activity · Global structure

1 Introduction

Solar activity is the most important modulation factor of ionosphere seasonal variations. Variations in solar wind and EUV radiation generated by solar rotation influence the earth ionosphere (Kutiev et al. 2012). Because of the non-uniform distribution and motion of EUV radiation sources, the EUV radiation reaches to the earth changes with the rotation of the sun. Because of the sun's rotation at its equator, the solar EUV radiation shows a seasonal variation of approximately 24–30 days (Pap et al. 1990; Kane 2002, 2003; Woods 2005; Ma et al. 2007). Bartels (1950) observed a period of approximately 27 days caused by solar radiation on an order of 6 to 10% in the noon values of foF2 for Huancayo, Peru. Titheridge (1973) studied the ionosphere electron content from June 1965 to August 1971 at latitudes of 34°S and 42°S and reported that the 27-day variations in the ionosphere follow the variations in solar flux with a delay of 1.0 ± 0.1 days. The signal of global mean TEC exhibits primary oscillations of 27-day, 0.5-, 1- and 11-year periods; there is a strong correlation between EUV radiation and global mean TEC in the 27-day oscillation, and the 13.5-day variation of EUV weakly correlates with 13.5-day variation of global mean TEC (Hocke 2008).

The F10.7 emission originates in the lower corona and chromosphere of the sun and has been a standard for solar activity in studies of the thermosphere and ionosphere (Viereck et al. 2001). The F10.7 index is used to repre-

✉ Yibin Yao
ybyao@whu.edu.cn

[1] School of Geodesy and Geomatics, Wuhan University, Wuhan, China

[2] Chinese Antarctic Center of Surveying and Mapping, Wuhan University, Wuhan, China

sent solar EUV radiation in many studies of the relationship between solar and ionospheric periodic modulations (e.g., Lei et al. 2008; Ma et al. 2012; Lee et al. 2012; Kutiev et al. 2012; Altadill and Apostolov 2003; Pancheva et al. 2002). Balan et al. (1994) and Liu et al. (2006) found that the F10.7 index exhibits a nonlinear relationship with solar EUV. Chen et al. (2011) found that the F10.7 index does not reflect the reduction in EUV radiation during the extended solar minimum of 2007 to 2009. F10.7 index may be not a perfect indicator of solar EUV radiation. Thus, there is a necessity to compare the coherence of F10.7 and SEM with solar EUV radiation in ionosphere variations.

Since coronal holes on the solar surface rotate with the sun, solar wind high-speed streams (HSS) that emanated from coronal holes will also cause repeated, temperate geomagnetic activities. If there is a large, isolated, near-equatorial coronal hole, the high-speed solar wind will interact/collide with the upstream slower-speed stream and form a corotating interaction region (CIR) (Tsurutani et al. 2006). Both, HSS and CIR generate temperate geomagnetic storms and continuous auroral activities, thereby generating 27-day variation in ionosphere.

There are rare magnetic storms generated by CIRs whose main phases intensity (in respect to Dst) are smaller than 100 nT. But nonlinear Alfvén waves (plasma oscillations in magnetized systems) within HSS can stretch the geomagnetic storms "recovery" phases to 27 days (Tsurutani et al. 2006). Apostolov et al. (2004) found that the evident increases of the 27-day oscillation could be distinguished in the foF2 and Ap variation sequences during the late declining phases of solar cycles, but the oscillations of F10.7 reduce gradually. In the geomagnetic disturbances, enormous solar wind energy is sedimented into the polar thermosphere. That generates the reduction in atoms-to-molecules ratio and the rise of the neutral gas temperature. Both of the changes contribute to a reduction in electron concentration in the high-latitude ionosphere (Danilov 2001).

Ma et al. (2012) investigated the contribution of EUV and geomagnetic activity at different latitudes and observed that at geomagnetic low latitudes, the contribution of EUV radiation was greater than geomagnetic activity. But geomagnetic activity has more prominent effect than EUV radiation at higher latitudes. Sagawa et al. (2005) found four peaks in longitudinal structure of equatorial anomaly in Far Ultraviolet (FUV) observations. Then, Immel et al. (2006) and England et al. (2006) provided mechanism interpretation with E-region non-migrating tide and noontime equatorial electrojet (EEJ) current density. There have not been many studies about 27-day variations that consider the earth as a whole, and it is necessary to study the global structure of 27-day variations of the ionosphere for the investigation of the relationship between geomagnetic field and ionosphere.

In this paper, we study the 27-day variation of the ionosphere and its relationship with solar EUV radiation and geomagnetic activity. The main goal is to present the 27-day variation of the ionosphere by time domain and analyze the contributions of solar EUV and geomagnetic activity with an emphasis on the difference between different geomagnetic latitudes. The global electron content (GEC), F10.7, SEM and Ap from 2000 to 2014 have been analyzed and filtered with the Chebyshev band-pass filter. Multiple linear regression was subsequently used to analyze the indices of SEM and F10.7 and contributions of solar EUV and geomagnetic activity. We employ the Chebyshev band-pass filter to filter the time series from 2000 to 2014 for all of the global ionosphere maps (GIM) grid points in order to obtain the global structure for 27-day variation of the ionosphere.

2 Data and methodology

2.1 Global ionosphere maps

The International GNSS Service (IGS) Ionosphere Working Group started to publish ionospheric TEC maps from June 1998. The TEC maps are generated from the weighted averages of the ionospheric products obtained by the independent calculation of the four analysis centers. Ionosphere climatology has recently been investigated on global and regional scales based on these long-term GPS TEC products (Liu et al. 2009; Lean et al. 2011). The characteristics of low-latitude TEC over the Indian sector are obtained using GIM data (1998–2014) filtering out the solar flare and storm effects, and long absence of winter anomaly is found (Dashora and Suresh 2015). Liu et al. (2014) calculated the Arctic mean TEC for the long-term prediction of the Arctic ionospheric TEC based on time-varying periodograms.

The global ionosphere maps used in the present work are generated by the Center for Orbit Determination in Europe (CODE) at the Astronomical Institute of the University of Bern (Hernández-Pajares et al. 2009). The TEC maps produced by CODE are modeled with spherical harmonic expansion up to degree 15 and order 15 with 3328 parameters referring to a solar-geomagnetic reference frame (http://aiuws.unibe.ch/ionosphere/). CODE provides TEC maps with a resolution of 5° in longitude, 2.5° in latitude, and 2 h in universal time. In this study, the TEC maps from June 1, 1999, until December 31, 2014, are used (ftp://ftp.unibe.ch/aiub/CODE/).

2.2 Global electron content

In recent years, a few indices have been proposed for the ionosphere climatology research such as the global mean TEC and global electron content (GEC). The parameter of GEC was

introduced by Afraimovich et al. (2006; 2008). It is defined as the total number of electrons in the near-earth space from the bottom of the ionosphere (60 km) to GPS satellites orbit (2000 km). The GEC is calculated by the summation of the values in each TEC maps cell multiplied by the cell area over all TEC maps cells (Afraimovich et al. 2006):

$$\begin{aligned} \mathrm{GEC} &= \sum_{i,j} I_{i,j} \cdot S_{i,j} \\ &= \sum_{i,j} I_{i,j} \cdot R_{\mathrm{E}}^2 \cdot \Delta\varphi \cdot [\sin\theta_j - \sin(\theta_j + \Delta\theta)] \end{aligned} \quad (1)$$

where $I_{i,j}$ is the value of indices i, j of TEC maps cell, R_{E} is the earth's radius, $\Delta\varphi$ and $\Delta\theta$ are the longitudinal and latitudinal region of the TEC maps cell, and φ_j and θ_j are the longitude and latitude of the cell. The authors suggested the GEC unit GECU $= 10^{32}$ electrons for convenience.

The estimation accuracy of GEC is higher than the accuracy of a single-cell value in TEC maps (5–20% Mannucci et al. 1998). GEC makes it possible to investigate the short-term and long-term state and variations of the ionosphere on a global scale.

2.3 SEM flux and F10.7 indices

The solar 10.7 cm radio flux has been continuously observed since 1947 by the National Research Council of Canada. The F10.7 cm flux originates in the lower corona and chromosphere of the sun and has been a standard for solar EUV radiation for the studies of thermosphere and ionosphere (Viereck et al. 2001). The Solar and Heliospheric Observatory (SOHO) was launched on December 2, 1995, and it is in a orbit around the sun–earth L1 Lagrange point. The Solar EUV Monitor (SEM) onboard SOHO has observed EUV with high temporal resolution (15 s) in three channels since December 1995. The first order of 26–34 nm flux is derived from channels 1 and 3, and the zero order of 0.1–50 nm flux is derived from channel 2 (Judge et al. 1998).

For comparison, we used both the F10.7 index and SEM flux data to analyze the 27-day variation of the ionosphere. The F10.7 data from January 1, 1999, to December 31, 2014, are downloaded from http://omniweb.gsfc.nasa.gov/form/dx1.html. The SEM data are downloaded from http://www.usc.edu/dept/space_science/semdatafolder/semdownload.htm. The daily average data of zero-order flux from March 1, 1999, to December 31, 2014, were chosen in this study (due to data gaps which occur before March 1, 1999).

2.4 Ap index

Ap index is a linearized geomagnetic index derived from a logarithmic Kp index through a one to one correspondence table. The Ap index is the daily average of Ap, and its values range from 0 to 400 with the unit 2 nT (Dieminger et al. 1996). The Ap index is determined from 13 stations at 46° to 63° north and south latitude, so it is able to represent the geomagnetic state of the whole earth. Ap index data are downloaded from http://omniweb.gsfc.nasa.gov/form/dx1.html. The time series from January 1, 1999, to December 31, 2014, is used in this study.

2.5 Data preprocessing

There are mainly two kinds of geomagnetic storms: CIR-generated and CME-generated geomagnetic storms. The CME-generated geomagnetic storms days need to be eliminated since it may influence the accuracy of the following study. We selected the days of Dst<-30 (Gonzalez et al. 1994) and further determined CME-generated geomagnetic storms days referring to Jian et al. (2006a, b). Ninety-two CME-generated geomagnetic storms corresponding to 177-day data were removed from original data (GIM, GEC, SEM, F10.7, Ap).

3 Results

3.1 Spectrum analysis

To illustrate the characteristics of periodic oscillations in the indices, we calculated the spectra of GEC, SEM, F10.7 and Ap index. The results are presented in Fig. 1. Notably, there is a prominent period peak of 27 days in all indices. The 27-day period in SEM and F10.7, which represent the solar EUV radiation, is attributed to the non-uniform distribution of EUV radiation sources as the sun rotates over a 27-day period (Pap et al. 1990; Kane et al. 2001; Kane 2002, 2003; Woods 2005; Ma et al. 2007). Coronal holes on the sun's surface can produce less EUV radiation than active regions; thus, the EUV flux will reduce when coronal holes face to the earth and the GEC will be modulated by the EUV variation directly (Xu et al. 2015). The Ap index also has 9-day and 13.5-day period peak. Temmer et al. (2007) suggested that the 9-day period is caused by a triangular distribution of CHs $\sim 120°$ apart in solar longitude and the 13.5-day period is generated by two CHs situated approximately 180° apart.

3.2 GEC_{27}

In digital signal processing, band-pass filters allow the desired frequency components to pass while attenuating the unwanted frequency components. Chebyshev band-pass filter has the property that they minimize the error between the idealized and the actual filter characteristic over the range of the filter, but with ripples in the passband (Wyndrum

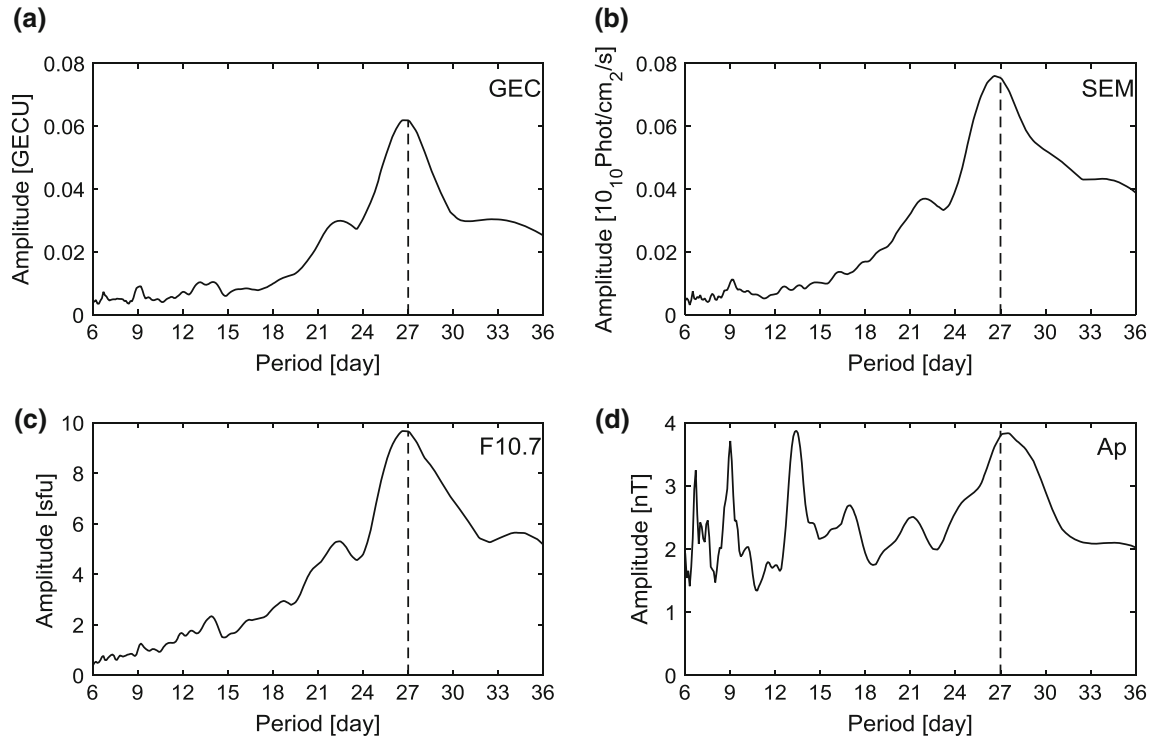

Fig. 1 Amplitude spectra of GEC, SEM, F10.7 and Ap in the period range from 6 to 36 days of 2008

1965; Rabiner 1976; Szentirmai 1982; Lyons 2011). Using the method described in the previous section, 2.2, we calculated the global electron content (Fig. 2, blue curve) and obtained the 27-day periodic component of GEC (GEC_{27}, Fig. 2, red curve) using a Chebyshev band-pass filter with the same period range as the solar EUV radiation shows (24 $\sim$ 30 days, Pap et al. 1990; Kane 2002, 2003; Woods 2005; Ma et al. 2007).

From 2000 to 2003, GEC value and GEC_{27} amplitude are both relatively large; from 2003 to 2009, with the decrease in GEC value, the amplitude of the GEC_{27} also decreases, reaching a minimum value; from 2009 to 2014, the amplitude of the GEC_{27} increases with the increase in GEC value. However, the amplitude of GEC_{27} is not always in exact agreement with the GEC value, such as the case in 2013 and 2014: The GEC value of 2013 is larger than 2014 while the amplitude of the GEC_{27} of 2013 is smaller than 2014. This is due to the variation of CIR.

We investigated the contribution of 27-day variation in the ionosphere during a 15-year period. The relative amplitude is defined as

$$G(i) = \sum_{j=(i-1)*27}^{i*27} \left| \frac{\mathrm{GEC}_{27}(j)}{\mathrm{GEC}(j)} \right| /27 \qquad (2)$$

Where $G(i)$ is relative amplitude; GEC(j) is the value of GEC at time j; $GEC_{27}(j)$ is value of 27-day periodic component of GEC at time j. An average of every 27 data are taken for showing the mean relative amplitude of every period. Figure 3 gives the relative magnitude of GEC_{27} in GEC. One can see that the contribution is prominent, varying from 1% to 17%. This indicates that the 27-day variations can be an important factor in the overall variations observed in the ionosphere.

3.3 A comparison of regression analysis accuracy of SEM flux and F10.7

A coherence comparison of the SEM and F10.7 with the ionosphere 27-day variation is shown in this section. We performed multiple linear regression analysis with the following formula:

$$\begin{aligned} \mathrm{mrGEC}_{27}(i) &= a + b\mathrm{SEM}_{27}(i - t_1) + c\mathrm{Ap}_{27}(i - t_2) \\ \mathrm{mrGEC}_{27}(i) &= a + b\mathrm{F10.7}_{27}(i - t_1) + c\mathrm{Ap}_{27}(i - t_2) \end{aligned} \qquad (3)$$

where mrGEC_{27} is the regression result of GEC_{27}; a, b and c are the regression coefficients; t_1 and t_2 are the time lags which range from 0 to 5, so there are 36 groups of regression and the minimum residuals group will be chosen as the time lags; the regression results show that the time lags of t_1 are typically 1 day and t_2 are typically 2 and 3 days; SEM_{27}, Ap_{27} and $F107_{27}$ are filtered in the range of periods from 24 to 30 days as the same as GEC_{27}. All time series of GEC_{27},

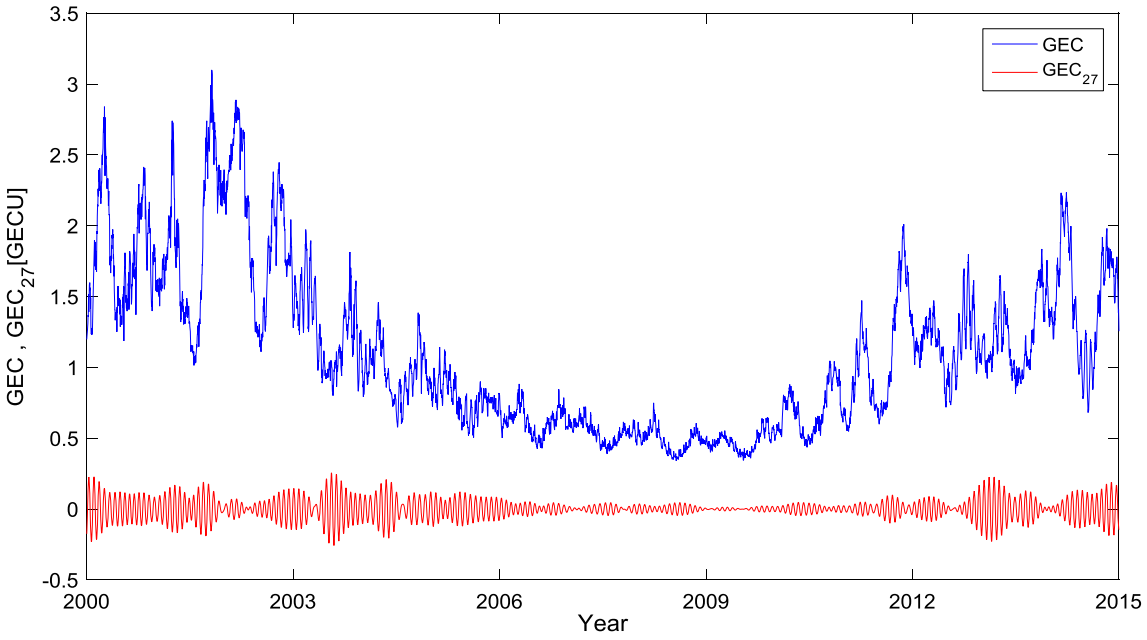

Fig. 2 GEC and GEC_{27} from 2000 to 2014

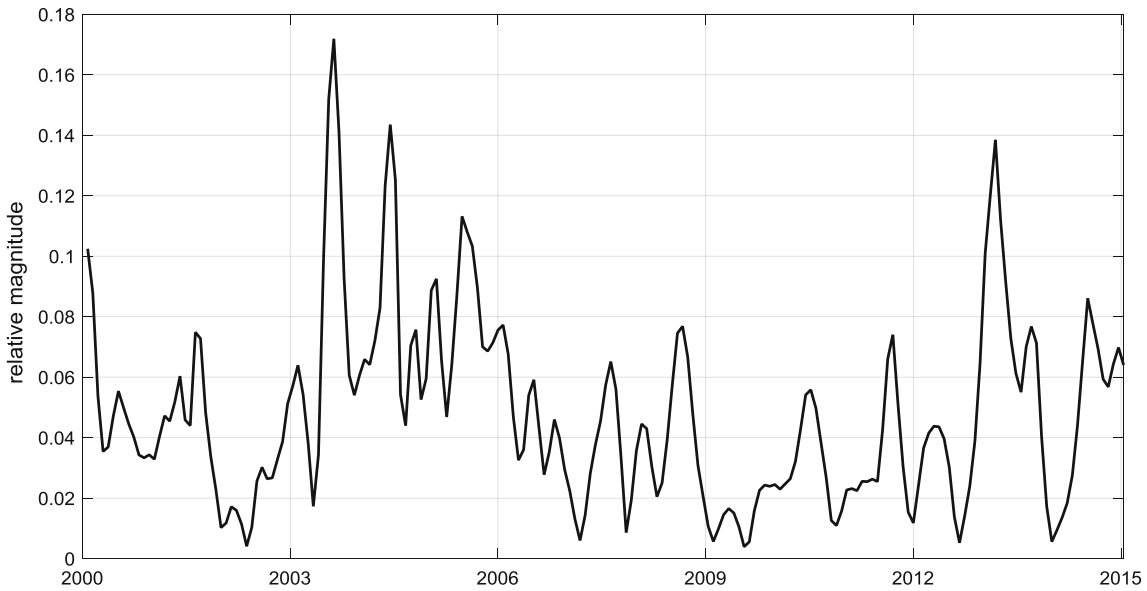

Fig. 3 Relative magnitude of GEC_{27} variations in GEC

SEM_{27}, Ap_{27} and $F10.7_{27}$ are normalized to [0,1] with the formula $X_i^{\text{norm}} = (X_i - X_{\min})/(X_{\max} - X_{\min})$. The multiple linear regression window is one year, which means the length of time series of GEC_{27}, $F10.7_{27}$, SEM_{27} and Ap_{27} is 365 or 366.

Figure 4 shows the multiple linear regression analysis results. The black lines are the original GEC27, and the red lines are the multiple linear regression analysis results. The left-hand column in Fig. 4 shows the regression results with SEM and Ap, and the right-hand column shows the regression results with F10.7 and Ap. It is clear that the regression results with SEM and Ap are better than with F10.7 and Ap, especially during the periods of day 1 to 150 day of 2001, day 250 to 365 of 2003, and day 150 to 250 of 2004.

Figure 5 shows the multiple linear regression residuals of SEM with Ap and F10.7 with Ap. We can see that the regression residuals of F10.7 with Ap varied from -0.2 to 0.25 and that the regression residuals of SEM with Ap varied from -0.15 to 0.15, which are notably smaller than F10.7 with Ap for the most part. Figure 6 shows the annual RMS multiple linear regression residuals of SEM with Ap (blue bars) and F10.7 with Ap (yellow bars). The RMS of regres-

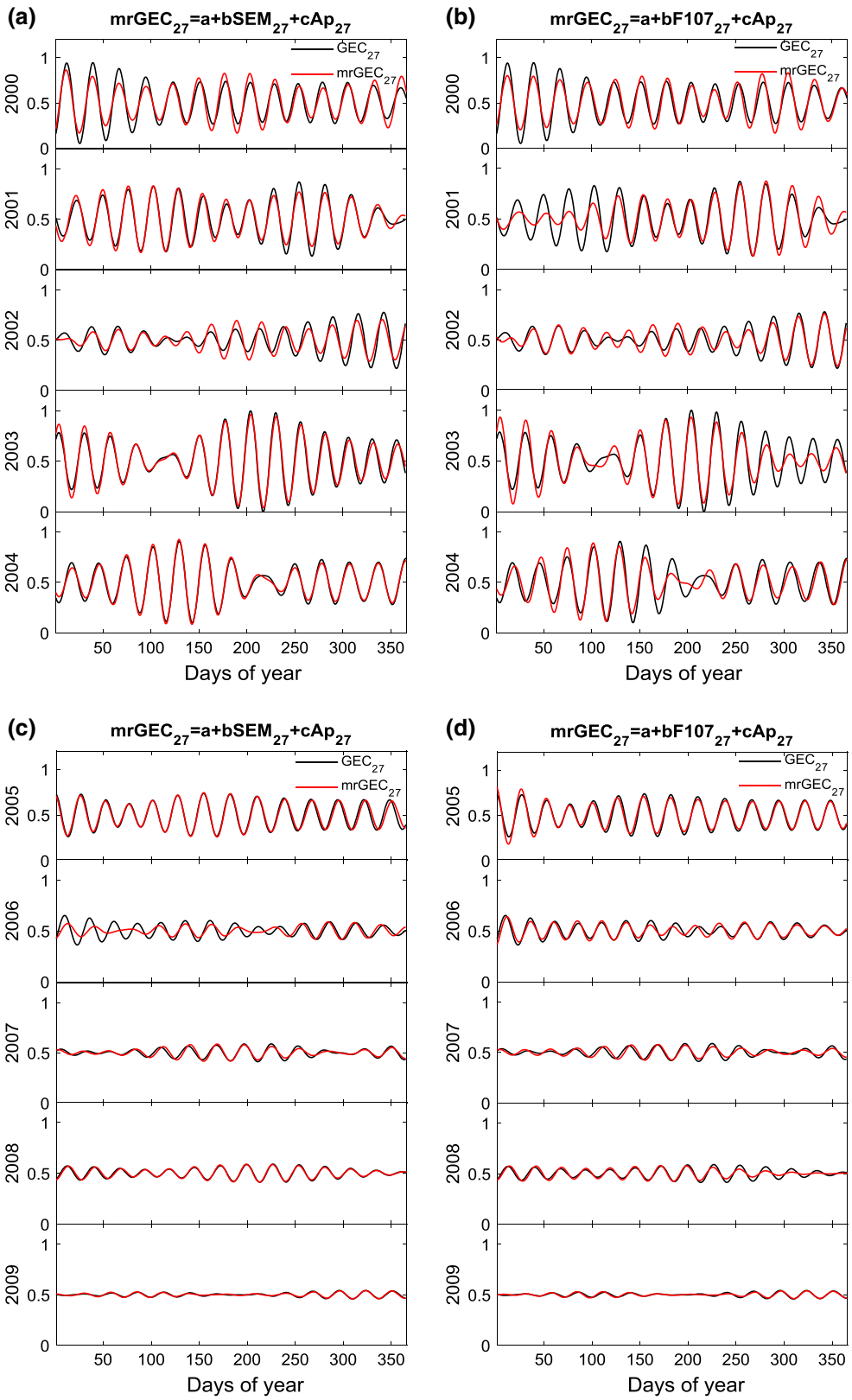

Fig. 4 Comparison of the multiple linear regression results between SEM with Ap and F10.7 with Ap

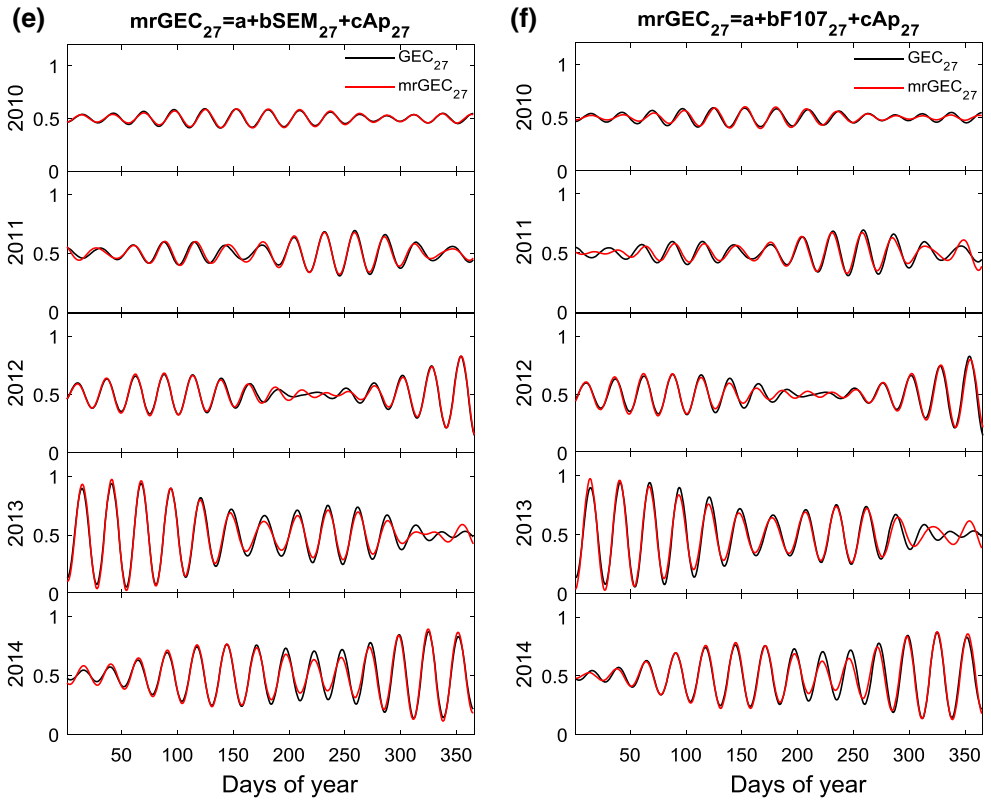

Fig. 4 continued

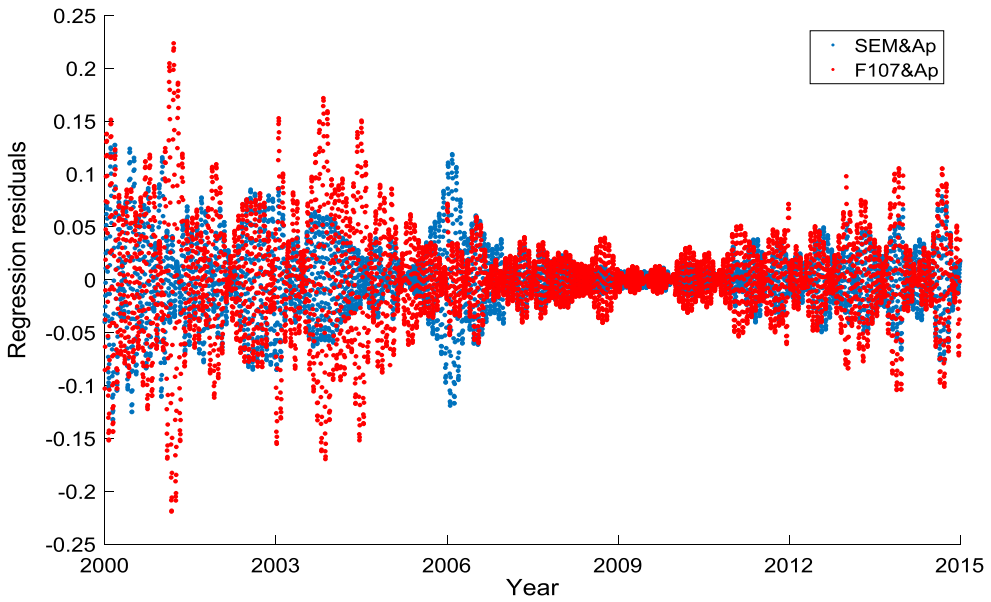

Fig. 5 Multiple linear regression residuals of SEM with Ap (*blue dots*) and F10.7 with Ap (*red dots*)

sion residuals of SEM with Ap is smaller than of F10.7 with Ap except 2006. It is clear that the SEM has a higher coherence than F10.7 for the 27-day variation of the ionosphere. So in the following study, we just use the SEM index representing the EUV radiation. The relatively large RMS value in 2006 of SEM is caused by the period difference between GEC_{27} and $mrGEC_{27}$ from December 2005 to October 2006, which means the observation of SOHO/SEM may be influenced by some factors during that time. During remarkably intense solar flares, the SEM measurements are saturated in

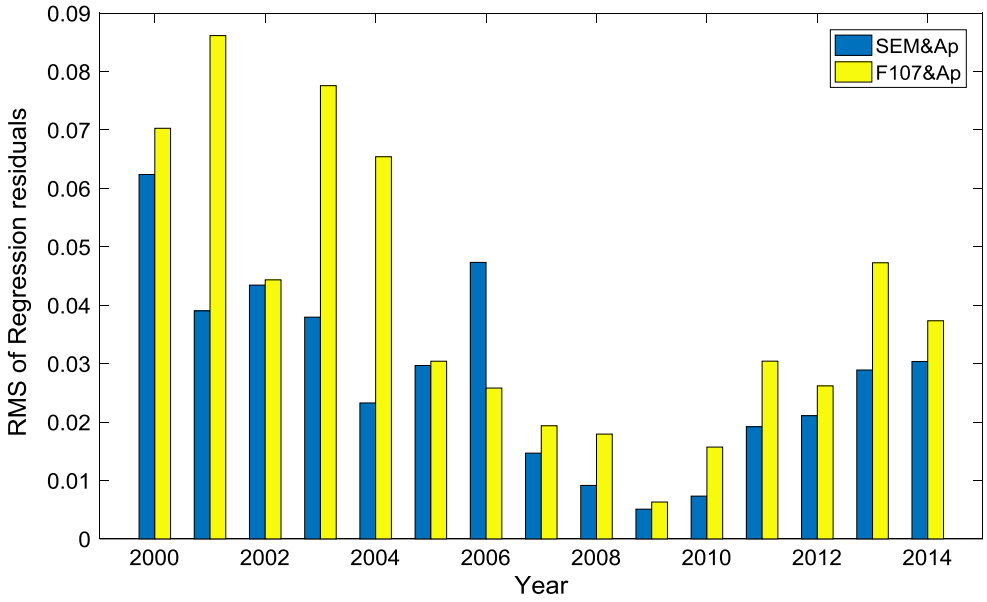

Fig. 6 Annual RMS multiple linear regression residuals of SEM with Ap (*blue bars*) and F10.7 with Ap (*yellow bars*)

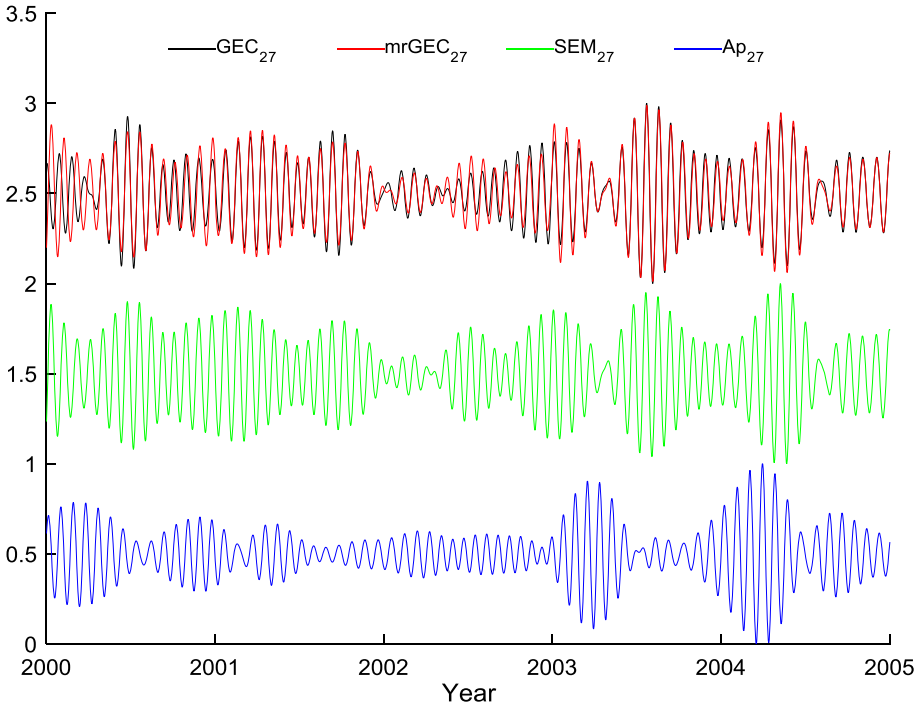

Fig. 7 Results of multiple linear regression, GEC_{27}, SEM_{27} and Ap_{27}

the zero-order channel and first-order channel is sensitive to the arrival of solar energetic particles (SEP) (Didkovsky et al. 2007; Hernández-Pajares et al. 2012). A revision of SEM measurements calibration is needed in the future study.

3.4 Contribution of EUV radiation and geomagnetic activity to 27-day variations of ionosphere

Figure 7 shows the results of multiple linear regression for GEC_{27}, SEM_{27} and Ap_{27} from 2000 to 2004. The feature that the two lines of original sequences (red) and regression sequences (black) are nearly overlapped indicate that the regression results reproduced the GEC_{27} well.

As we can see, comparing the variations of SEM_{27}, Ap_{27} with GEC_{27}, the EUV radiation seasonal variations are the main driver for the 27-day variations of the ionosphere over most periods.

Figure 8 shows the regression ratios of SEM_{27} and Ap_{27}. The regression coefficients of SEM_{27} varied from 0.6 to 1.4 which indicates that the EUV radiation seasonal variations

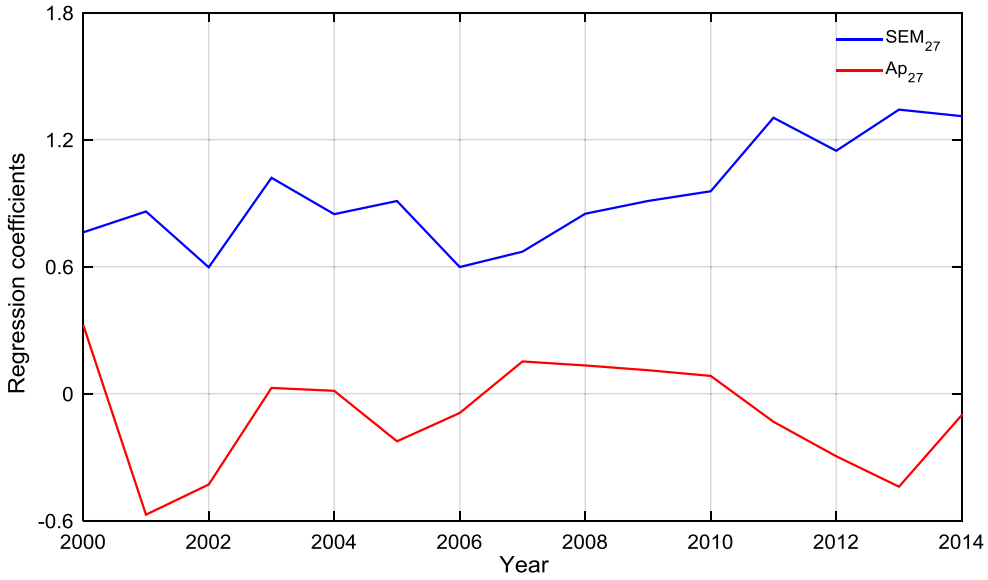

Fig. 8 Regression coefficients of SEM_{27} and Ap_{27}

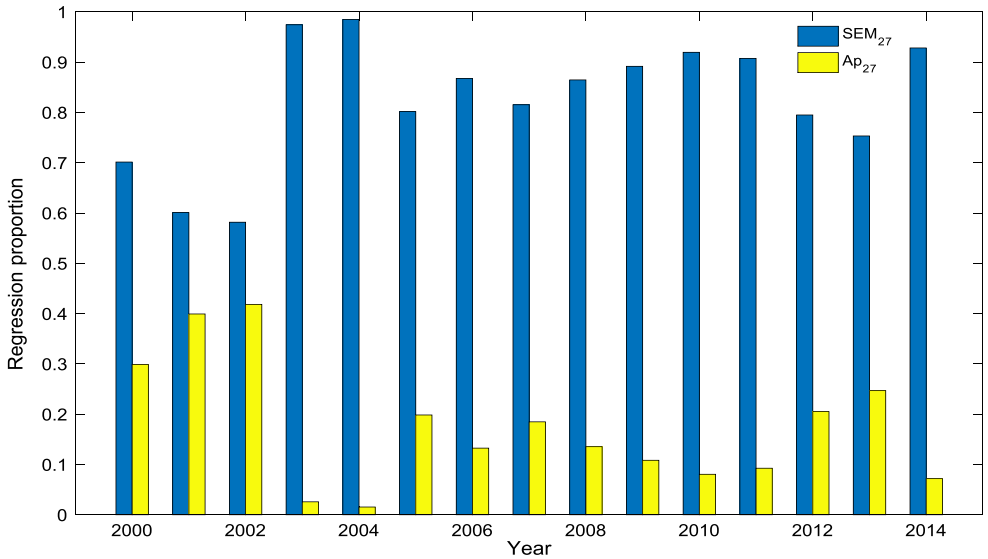

Fig. 9 Regression proportion of SEM_{27} and Ap_{27}

are the primary positive process. The coefficients of Ap_{27} varied from -0.6 to 0.3 which suggests that geomagnetic activity is a secondary factor and characteristics of its process vary with time.

We calculated the regression proportion of SEM_{27} and Ap_{27} with the following formula:

$$\begin{aligned} \text{SEM}_{27}\ \text{proportion} &= \frac{|b|}{|b|+|c|} \\ \text{Ap}_{27}\ \text{proportion} &= \frac{|c|}{|b|+|c|} \end{aligned} \tag{4}$$

where b and c are the regression coefficients. Figure 9 shows the bar chart of regression proportion of SEM_{27} (blue bars) and yellow bars). The regression proportion of SEM_{27} varied from 60 to 98%, and the Ap_{27} varied from 2 to 40%. The bar chart further illustrates that EUV radiation seasonal variations are the main driver for 27-day variation of the ionosphere.

For the investigation of the contribution of solar EUV radiation and geomagnetic activity in the ionosphere to 27-day variation at different latitudes, we chose TEC map cells on three meridians (70°W, 30°E, 145°E, latitude from 70°N to 70°S), where IGS stations are dense. There are 57 cells on a meridian as the resolution of TEC map on latitude is 2.5° and there is a 15-year time series of every cell. Using the same regression method described earlier, we calculated the mean regression ratios of the 15 years of every cell on the three

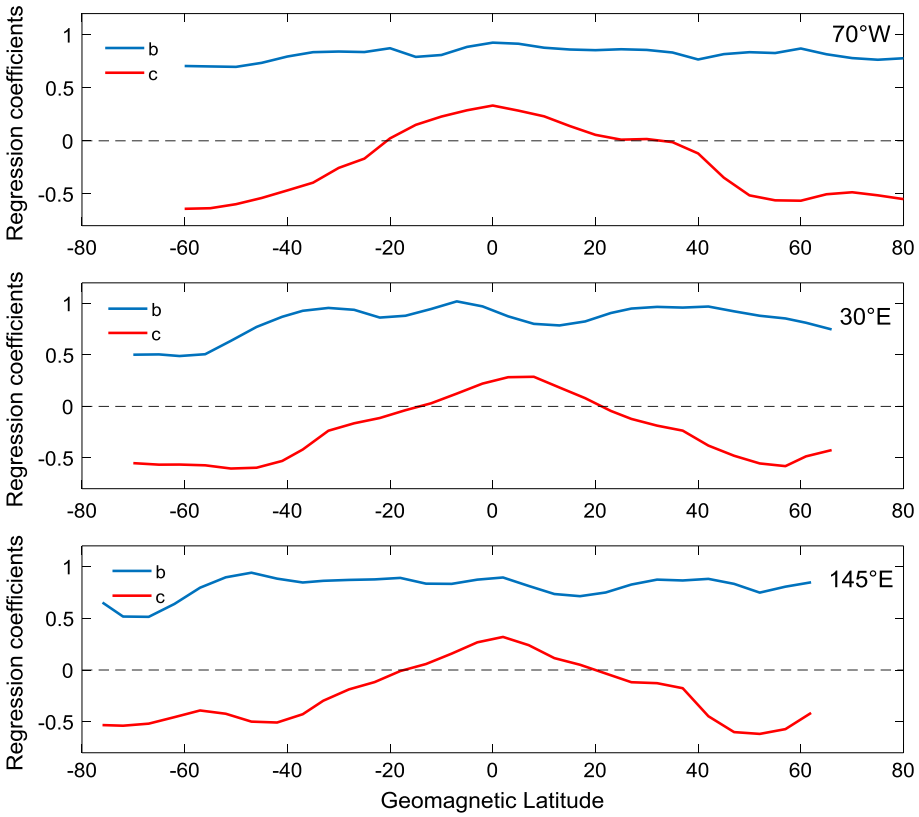

Fig. 10 Regression coefficients of three meridians, *b* (*blue lines*) is SEM_{27} regression coefficient and *c* (*red lines*) is Ap_{27} regression coefficients

meridians. Figure 10 shows the regression coefficients of the three meridians. The regression coefficient *b* (blue lines) and *c* (red lines), respectively, represents the contribution of solar EUV radiation and geomagnetic activity on ionosphere 27-day variation. As we can see, the regression coefficient *b* varied from 0.5 to 0.9 and there is little variation with geomagnetic latitude, which indicates that the relationship between EUV radiation and ionosphere 27-day variations is positive. However, *c* varies from −0.7 to 0.3 and the shape of the curve is generally symmetrical about the magnetic equator. The values of cat high geomagnetic latitudes are negative and increase with geomagnetic latitudes becoming lower, reaching 0 at approximately 20° (north and south) and reaching the maximum at the geomagnetic equator.

3.5 Global structure of 27-day variations of ionosphere

To investigate the global structure of 27-day variations of ionosphere, the Chebyshev band-pass filter is applied to get TEC_{27} time series of every grid point in global ionospheric maps from their 15 years' TEC time series. Then, the TEC_{27} daily average magnitude map is obtained by averaging every grid point's TEC_{27} time series. Figure 11 shows the TEC_{27} daily average magnitude global structure of 2000–2014. The two red lines in Fig. 11 indicate 20 and −20 geomagnetic latitudes of corrected geomagnetic coordinates (CGM). One can see that there are two prominent zonal anomaly regions along with the geomagnetic latitudes lines. Additionally, there are two peaks of zonal anomaly regions (white ellipses) from 110°E to 140°W at the symmetry locations of magnetic equator where the TEC_{27} magnitude values are obvious larger than elsewhere along the zonal anomaly regions.

4 Discussion

The relationship between solar EUV flux and 27-day variation of the ionosphere is always positive, but the effect of geomagnetic activity on the ionosphere is negative at high and middle geomagnetic latitude and becomes positive at low geomagnetic latitudes (Fig. 10). Emitted HSS from Coronal holes can generate a series of temperate weak geomagnetic storms that can last more than one solar rotation. And when HSS collide with low-speed solar wind, CIRs will form and induce magnetic activity. All these recurrent geomagnetic activities induced by solar rotation can perturb ionosphere with a 27-day period.

During CIR-induced magnetic storms, enormous solar wind energy is sedimented into the thermosphere at high latitudes. This phenomenon leads to reduction in the atoms-to-molecules ratio and an increase of the neutral gas temperature. These two factors can generate the electron concentration reduction in the high-latitude ionosphere (Danilov 2001). The gas with depleted $[O]/[N_2]$ cannot be brought to a

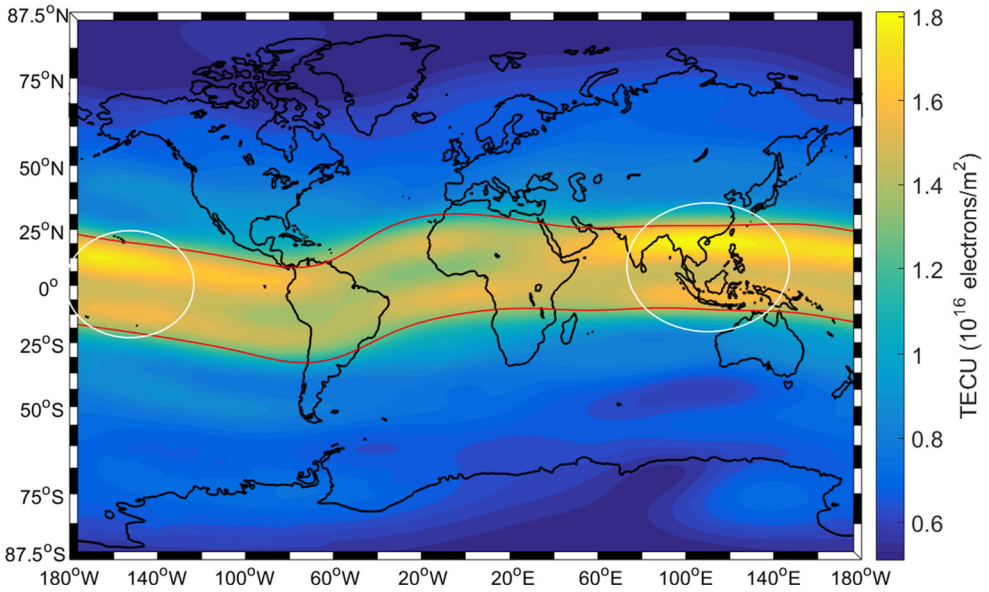

Fig. 11 TEC_{27} daily average magnitude of 2000–2014

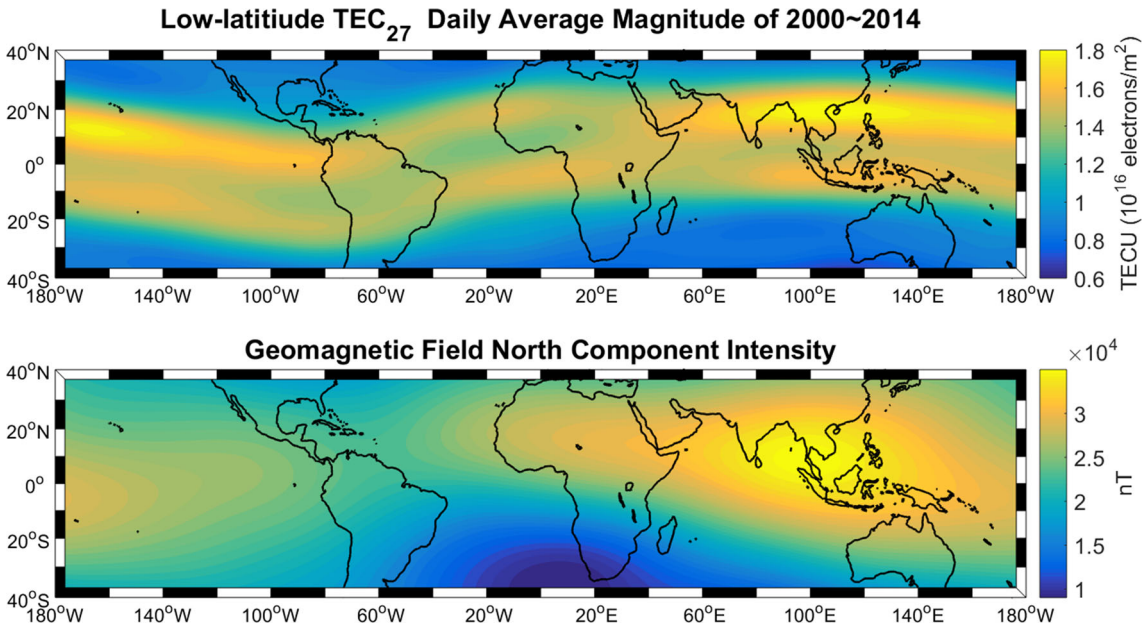

Fig. 12 Comparison of low-latitude TEC_{27} daily average magnitude and geomagnetic field north component

lower latitude and the negative phases cannot spread equatorward; thus, the negative phases are "locked" in the high and middle latitudes (Prölss 1995; Danilov 2001; Rishbeth 1998; Rishbeth and Mendillo 2001; Wang et al. 2010; Astafyeva et al. 2015). So the recurrent geomagnetic activities have stronger negative effect on ionosphere at high latitude and weaker positive effect at low latitude as Fig. 10 shows.

The eastward electric fields in E layer can penetrate into F layer. The equatorial plasma upwells by $\mathbf{E} \times \mathbf{B}$ force and turns downward with magnetic field lines causing two crests around $\pm 12°$–$15°$ magnetic latitudes. This process is known as fountain effect (Tanaka 1986; Batista et al. 1991; Greenspan et al. 1991). The zonal TEC_{27} peaks are caused by the fountain effect, and the anomaly region may be induced by the non-uniform geomagnetic field structures. Figure 12 shows the comparison of the low-latitude TEC_{27} daily average magnitude and the geomagnetic field north component. One can clearly see that the intensity of the geomagnetic field north component in the north of Southeast Asia and Middle Pacific is conspicuous higher than elsewhere. As a result, more electrons are diffused to the anomaly region by the $\mathbf{E} \times \mathbf{B}$ drift because of the larger inten-

sity of the geomagnetic field in Southeast Asia and Middle Pacific.

5 Conclusions

In this study, the global electron content was used to represent the global ionosphere variation, and a Chebyshev band-pass filter was used to obtain the time series of GEC_{27}, SEM_{27}, $F10.7_{27}$ and Ap_{27}. A coherence comparison of SEM and F10.7 with the ionosphere 27-day variation was calculated using multiple linear regression analysis. We also explored the contribution of EUV radiation and geomagnetic activity to 27-day variations of the ionosphere using the SEM and Ap indices. Additionally, global structure of 27-day variations of the ionosphere was demonstrated and analyzed in part. The main conclusions drawn are as follows:

1. There are dominant periods near 27 days in GEC, SEM, F10.7 and Ap (Fig. 1). The values of GEC varied from 0.5 to 3.2 GECU (Fig. 2) and the amplitude of GEC_{27} agree with the values of GEC. The relative magnitude of GEC_{27} in GEC varied from 1 to 17% (Fig. 3).
2. The multiple linear regression results are both good for $F10.7_{27}$ with Ap_{27}, and for SEM_{27} with Ap_{27} (Fig. 4). However, the regression residuals of $F10.7_{27}$ with Ap_{27} are larger than for SEM_{27} with Ap_{27} (Figs. 5, 6). The SEM has a higher coherence with the 27-day variation of the ionosphere than F10.7. The EUV radiation seasonal variations are the main driver for the 27-day variations of the ionosphere in most periods.
3. The regression coefficients of SEM_{27} of three meridians varied from 0.5 to 0.9, and there is little variation with geomagnetic latitudes, which indicates that the relationship between EUV radiation and ionosphere 27-day variations is positive and that there is rarely a difference at different latitudes. The regression coefficients of Ap_{27} are negative at high geomagnetic latitudes, increasing with decreasing geomagnetic latitudes, becoming positive at low geomagnetic latitudes. The relationship between geomagnetic activity and ionosphere 27-day variations is negative at high and middle geomagnetic latitudes and positive at low geomagnetic latitudes.
4. There are two zonal anomaly regions along with the geomagnetic latitudes lines caused by the fountain effect. Two peaks (white ellipses) from 110°E to 140°W at the symmetry locations of magnetic equator are found, and this may be induced by the non-uniform geomagnetic field structures as the intensity of the geomagnetic field north component in the north of Southeast Asia and the Middle Pacific is conspicuous higher than elsewhere.

Acknowledgements The authors would like to express their gratitude to Center for Orbit Determination in Europe (CODE) for TEC maps. The F10.7 and Ap indices data are available through http://omniweb.gsfc.nasa.gov/form/dx1.html, and the SEM data are downloaded from http://www.usc.edu/dept/space_science/semdatafolder/semdownload.htm. This work was supported by the General Program of National Natural Science Foundation of China (No. 41274022, 41574028) and the Natural Science Foundation for Distinguished Young Scholars of Hubei Province of China (No. 2015CFA036).

References

Afraimovich EL, Astafyeva EI, Zhivetiev IV (2006) Solar activity and global electron content. Doklady Earth Sci 409(2):921–924. doi:10.1134/S1028334X06060195

Afraimovich EL, Astafyeva EI, Oinats AV, Yasukevich YV, Zhivetiev IV (2008) Global electron content: a new conception to track solar activity. Ann Geophys 26(2):335–344

Altadill D, Apostolov EM (2003) Time and scale size of planetary wave signatures in the ionospheric F region: role of the geomagnetic activity and mesosphere/lower thermosphere winds. J Geophys Res Space Phys (1978–2012) 108(A11):45

Apostolov EM, Altadill D, Todorova M (2004) The 22-year cycle in the geomagnetic 27-day recurrences reflecting on the F2-layer ionization. Ann Geophys 22(4):1171–1176. doi:10.5194/angeo-22-1171-2004

Astafyeva E, Zakharenkova I, Förster M (2015) Ionospheric response to the 2015 St. Patrick's Day storm: a global multi-instrumental overview. J Geophys Res Space Phys 120(10):9023–9037. doi:10.1002/2015JA021629

Balan N, Bailey GJ, Jenkins B, Rao PB, Moffett RJ (1994) Variations of ionospheric ionization and related solar fluxes during an intense solar cycle. J Geophys Res Atmos 99(A2):2243–2253. doi:10.1029/93JA02099

Bartels J (1950) 27-day variations in F2 layer critical frequencies at Huancayo. J Atmos Terr Phys 1(1):2–12. doi:10.1016/0021-9169(50)90010-9

Batista IS, de Paula ER, Abdu MA, Trivedi NB (1991) Ionospheric effects of the March 13, 1989, magnetic storm at low and equatorial latitudes. J Geophys Res 96:13,943–13,952

Chen Y, Liu L, Wan W (2011) Does the $F_{10.7}$ index correctly describe solar EUV flux during the deep solar minimum of 2007–2009? J Geophys Res Space Phys 116(A4):1451–1453

Danilov AD (2001) F2-region response to geomagnetic disturbances. J Atmos Sol Terr Phys 63(5):441–449. doi:10.1016/S1364-6826(00)00175-9

Dashora N, Suresh S (2015) Characteristics of low-latitude TEC during solar cycles 23 and 24 using global ionospheric maps (GIMs) over Indian sector. J Geophys Res Space Phys 120(6):5176–5193

Didkovsky LV, Judge DL, Jones AR, Wieman S, Tsurutani BT, Mcmullin D (2007) Correction of SOHO CELIAS/SEM EUV measurements saturated by extreme solar flare events. Astron Nachr 328(1):36–40

England SL, Maus S, Immel TJ, Mende SB (2006) Longitudinal variation of the E-region electric fields caused by atmospheric tides. Geophys Res Lett 33:L21105. doi:10.1029/2006GL027465

Gonzalez WD, Joselyn JA, Kamide Y, Kroehl HW, Rostoker G, Tsurutani BT, Vasyliunas VM (1994) What is a geomagnetic storm? J Geophys Res Space Phys 99(A4):5771–5792

Greenspan ME, Rasmussen CE, Burke WJ, Abdu MA (1991) Equatorial density depletion observed at 840 km during the great magnetic storm of March 1989. J Geophys Res 96:13,931–13,942

Hernández-Pajares M, Juan JM, Sanz J, Orus R, Garcia-Rigo A, Feltens J, Krankowski A (2009) The IGS VTEC maps: a reliable source of ionospheric information since 1998. J Geod 83(3–4):263–275

Hernández-Pajares M, García-Rigo A, Juan JM, Sanz J, Monte E, Aragón-Àngel A (2012) GNSS measurement of EUV photons flux rate during strong and mid solar flares. Space Weather 10(12):1702–1711

Hocke K (2008) Oscillations of global mean TEC. J Geophys Res Space Phys 113(A4). doi:10.1029/2007JA012798

Immel TJ, Sagawa E, England SL, Henderson SB, Hagan ME, Mende SB, Frey HU, Swenson CM, Paxton LJ (2006) Control of equatorial ionospheric morphology by atmospheric tides. Geophys Res Lett 33:L15108. doi:10.1029/2006GL026161

Jian L, Russell CT, Luhmann JG, Skoug RM (2006) Properties of interplanetary coronal mass ejections at one au during 1995–2004. Sol Phys 239(1):393–436

Jian L, Russell CT, Luhmann JG, Skoug RM (2006) Properties of stream interactions at one au during 1995–2004. Sol Phys 239(1):337–392

Judge DL, Mcmullin DR, Ogawa HS, Hovestadt D, Klecker B, Hilchenbach M et al (1998) First solar EUV irradiances obtained from SOHO by the CELIAS/SEM. Solar Phys 177(1):161–173

Kane RP, Vats HO, Sawant HS (2001) Short-term periodicities in the time series of solar radio emissions at different solar altitudes. Sol Phys 201:181–190. doi:10.1023/A:1010349014498

Kane RP (2002) Variability in the periodicity of 27 day in solar indices. Sol Phys 209:207–216. doi:10.1023/A:1020959817176

Kane RP (2003) Solar EUV and ionospheric parameters: a brief assessment. Adv Space Res 32:1713–1718. doi:10.1016/S0273-1177(03)90467-4

Kutiev I, Otsuka Y, Pancheva D, Heelis R (2012) Response of low-latitude ionosphere to medium-changes of solar and geomagnetic activity. J Geophys Res Space Phys (1978–2012) 117(A8):3

Lean JL, Meier RR, Picone JM, Emmert JT (2011) Ionospheric total electron content: global and hemispheric climatology. J Geophys Res Space Phys 116(A10). doi:10.1029/2011JA016567

Lee CK, Han SC, Bilitza D, Seo KW (2012) Global characteristics of the correlation and time lag between solar and ionospheric parameters in the 27-day period. J Atmos Sol Terr Phys 77(219–224):1

Lei J, Thayer JP, Forbes JM, Sutton EK, Nerem RS (2008) Rotating solar coronal holes and periodic modulation of the upper atmosphere. Geophys Res Lett 35(10):105

Liu L, Wan W, Ning B, Pirog OM, Kurkin VI (2006) Solar activity variations of the ionospheric peak electron density. J Geophys Res Space Phys (1978–2012) 111(A8):133. doi:10.1029/2006JA011598

Liu L, Wan W, Ning B, Zhang ML (2009) Climatology of the mean total electron content derived from GPS global ionospheric maps. J Geophys Res Space Phys 114(A6). doi:10.1029/2009JA014244

Liu J, Chen R, Wang Z, An J, Hyyppä J (2014) Long-term prediction of the Arctic ionospheric TEC based on time-varying periodograms. PloS One 9(11):e111497

Lyons RG (2011) Understanding digital signal processing, 3rd edn. Pearson Education, India

Ma R, Ji Q, Xu J (2007) Wavelet analysis of 27-day oscillations in the solar index F10.7 (in Chinese). Chin J Space Sci 27:89–95

Ma R, Xu J, Wang W, Lei J (2012) The effect of $\sim$ 27 day solar rotation on ionospheric F2 region peak densities (NmF2). J Geophys Res Space Phys (1978–2012) 117(A3):12

Mannucci AJ, Wilson BD, Yuan DN, Ho CH, Lindqwister UJ, Runge TF (1998) Global mapping technique for GPS-derived ionospheric total electron content measurements. Radio sci 33(3):565–582

Pancheva D, Mitchell N, Clark RR, Drobjeva J, Lastovicka J (2002) Variability in the maximum height of the ionospheric F2-layer over Millstone Hill (September 1998? March 2000); influence from below and above. Ann Geophys 20(11):1807–1819

Pap J, Tobiska WK, Bouwer SD (1990) Periodicities of solar irradiance and solar activity indices, I. Sol Phys 129:165–189. doi:10.1007/BF00154372

Prölss GW (1995) Ionospheric F region storms. In: Volland H (ed) Handbook of atmospheric electrodynamics, vol 2. CRC Press, Boca Raton, pp 195–248

Rabiner L (1976) Approximation methods for electronic filter design. IEEE Trans Acoust Speech Signal Process 24(4):346–346

Rishbeth H (1998) How the thermospheric circulation affects the ionospheric F2-layer. J Atmos Sol Terr Phys 60:1385–1402. doi:10.1016/S1364-6826(98)00062-5

Rishbeth H, Mendillo M (2001) Patterns of F2-layer variability. J Atmos Sol Terr Phys 63:1661–1680. doi:10.1016/S1364-6826(01)00036-0

Sagawa E, Immel TJ, Frey HU, Mende SB (2005) Longitudinal structure of the equatorial anomaly in the nighttime ionosphere observed by IMAGE/FUV. J Geophys Res 110:A11302. doi:10.1029/2004JA010848

Szentirmai G (1982) Electronic filter design handbook. Proc IEEE 70(3):317–317

Tanaka T (1986) Low-latitude ionospheric disturbances: results for March 22, 1979, and their general characteristics. Geophys Res Lett 13:1399–1402

Temmer M, Vršnak B, Veronig AM (2007) Periodic appearance of coronal holes and the related variation of solar wind parameters. Sol Phys 241(2):371–383. doi:10.1007/s11207-007-0336-1

Titheridge JE (1973) The electron content of the southern mid-latitude ionosphere, 1965–1971. J Atmos Terr Phys 35(5):981–1001. doi:10.1016/0021-9169(73)90077-9

Tsurutani BT, Gonzalez WD, Gonzalez AL, Guarnieri FL, Gopalswamy N, Grande M,. & McPherron, R. (2006) Corotating solar wind streams and recurrent geomagnetic activity: a review. J Geophys Res Space Phys 111(A7). doi:10.1029/2005JA011273

Viereck R, Puga L, McMullin D, Judge D, Weber M, Tobiska WK (2001) The Mg II index: a proxy for solar EUV. Geophys Res Lett 28(7):1343–1346

Wang W, Lei J, Burns AG, Solomon SC, Wiltberger M, Xu J, Zhang Y, Paxton L, Coster A (2010) Ionospheric response to the initial phase of geomagnetic storms: common features. J Geophys Res 115:A07321. doi:10.1029/2009JA014461

Woods TN et al (2005) Solar EUV experiment (SEE): mission overview and first results. J Geophys Res 110:A01312. doi:10.1029/2004JA010765

Wyndrum RW (1965) Microwave filters, impedance-matching networks, and coupling structures. Proc IEEE 53(7):766–766

Xu J, Wang W, Zhang S, Liu X, Yuan W (2015) Multiday thermospheric density oscillations associated with variations in solar radiation and geomagnetic activity. J Geophys Res Space Phys 120(5):3829–3846. doi:10.1002/2014JA020830